Intensity difference squeezing in a strongly overcoupled silicon nitride microresonator

Optics Letters

Intensity difference squeezing in a strongly overcoupled silicon nitride microresonator

Sara Persia,[1,*] Yi Sun,[1] Vaishali Adya,[2] and Victor Torres-Company[1]

[1]Department of Microtechnology and Nanoscience, Chalmers University of Technology, SE-41296 Göteborg, Sweden
[2]Department of Applied Physics, KTH Royal Institute of Technology, SE-106 91 Stockholm, Sweden
*persias@chalmers.se

Received 16 January 2026; revised 2 April 2026; accepted 7 April 2026; posted 7 April 2026; published 8 May 2026

Integrated nonlinear microring resonators are promising sources of bright twin-beams exhibiting intensity difference squeezing. To take advantage of the noise reduction of these quantum states, many applications require high squeezing levels. However, the attainable on-chip squeezing is constrained by the ratio of intrinsic to coupling loss, which is strongly related to design and fabrication limits. Here, we demonstrate a silicon nitride microring resonator engineered to enable a set of periodic strongly overcoupled resonances from which the estimated on-chip intensity difference squeezing is 11.8 dB, exceptionally high for an integrated device. Due to significant setup loss, we directly measure 1.4 ± 0.2 dB of squeezing, corresponding to an on-chip level of 9.2 ± 5.1 dB. In addition, the new, to the best of our knowledge, design inherently suppresses mode competition in the modes surrounding the twin-beams, enabling a constant high squeezing level up to moderate powers. These results represent a significant step toward the miniaturization of integrated devices whose performance benefits from surpassing the quantum noise limit using squeezed states, with particular relevance to sensing applications.

https://doi.org/10.1364/OL.590513

The main characteristic of squeezed states of light is the reduction of noise in one quadrature of a conjugate pair below the quantum noise limit of the vacuum state [1]. This nonclassical property offers significant technological advantages in several fields of research, from continuous-variable quantum computing [2,3] to sensing [4] and spectroscopy [5]. The most relevant example is the increased sensitivity achieved at the laser interferometer gravitational-wave observatory, where bulk optical cavities are employed to generate and control frequency-dependent squeezed vacuum states [6,7]. So far, high levels of squeezing have been demonstrated mainly in bulk systems [8–10], with the current record of 15 dB obtained from a periodically poled KTP crystal-based optical parametric amplifier (OPA) [11].

Nevertheless, growing interest is directed toward the use of photonic integrated circuits (PICs) as squeezing sources because of their advantages in scalability, small footprint, and low power consumption. Since squeezed states require a nonlinear process to be generated, χ^2 and χ^3 nonlinear materials are commonly used in PICs devices, such as thin film lithium niobate ($LiNbO_3$) OPAs [12,13] and silicon nitride (Si_3N_4) optical parametric oscillators (OPOs). In particular, because of their low propagation loss, strong χ^3 nonlinearity, and compatibility with complementary metal-oxide semiconductor (CMOS) technology, Si_3N_4 microring resonators have been widely employed to generate squeezed vacuum [14–17], quantum squeezed combs [18–21], and intensity difference squeezing [14,22–26].

The latter is produced by pumping an OPO above the oscillation threshold P_{th}, enabling the growth of new frequency modes generated in signal-idler pairs according to the four-wave mixing (FWM) process. These bright twin-beams exhibit intensity difference noise below the vacuum noise level [27,28]. This type of squeezing is especially promising in sensing applications, where higher sensitivity is usually reached by increasing the power of the probe laser. By using intensity difference squeezing, it is possible to further improve the sensitivity and the signal-to-noise ratio for a fixed power level [4,29–34].

The detectable intensity difference squeezing level generated in Si_3N_4 microresonators is [27]:

$$S = 10 \log_{10}(1 - \eta_{\mathrm{path}} \eta_{\mathrm{D}} \theta), \tag{1}$$

where η_{path} and η_{D} are the path and detection quantum efficiencies, respectively, and $\theta = 1 - \frac{Q_{\mathrm{L}}}{Q_{\mathrm{i}}}$ is the overcoupling coefficient, with Q_{L} and Q_{i} being the loaded and intrinsic quality factors. Equation (1) is valid when the product between the photon cavity lifetime τ_{c} and the measurement sideband frequency Ω is $\tau_{\mathrm{c}}\Omega \ll 1$. The achievable on-chip squeezing $S_{\text{on-chip}}$, obtained from Eq. (1) with $\eta_{\mathrm{path}} = \eta_{\mathrm{D}} = 1$, depends exclusively on the ratio of intrinsic to extrinsic quality factors ($Q_{\mathrm{i}}/Q_{\mathrm{e}}$), which is maximized in the strongly overcoupled regime $Q_{\mathrm{i}}/Q_{\mathrm{e}} \gg 1$, where propagation losses are much lower than coupling losses [27]. Reaching this regime is nontrivial because of fabrication limits. A small Q_{e} is achieved by reducing the ring-bus waveguide gap. However, difficulties in controlling the aperture of such small gaps lead to an increase in the total intrinsic loss due to higher sidewall roughness [35]. On the other hand, a large Q_{i} is not only necessary for optimal squeezing generation, but also to reduce the oscillation threshold and to ensure strong parametric gain.

Keeping high Q_i and low Q_e at the same time is therefore challenging. A further limitation in typical high Q_i resonators is the onset of oscillations of several frequency modes from high-order FWM even at moderate pump power. This causes mode competition and therefore reduces the maximum power that twin-beams can sustain while maintaining high levels of squeezing. Similar issues for high Q_i microrings operating in the classical regime have previously been overcome in our group by engineering the microring design so that periodic supermodes with an extremely high Q_i/Q_e ratio can be created [35,36]. In this Letter, we use the strongly overcoupled resonances of these devices to show an on-chip intensity difference squeezing of 9.2 dB from twin-beams that can potentially reach a few mW of on-chip power while maintaining low power in the secondary modes and suppressing the oscillations of all other frequency modes.

For this demonstration, we fabricate a Si_3N_4 microresonator embedded in SiO_2 using a subtractive process [37,38]. The ring has a radius of 227.8 μm, corresponding to a free spectral range (FSR) of 100 GHz. As shown in the schematic in Fig. 1(a), both the ring and the bus waveguide have a cross section of $740 \times 2400\ nm^2$, supporting the fundamental TE_{00} mode as well as the higher-order modes TE_{10} and TE_{20}. The latter can be neglected due to their low quality (Q) factors. The bus waveguide ends are tapered to ensure excitation of only the TE_{00} mode and to improve fiber-to-chip coupling. The gap between the bus and the ring waveguides is reduced to 120 nm. This small separation enables the coupling between the fundamental cavity mode and both guided and radiation modes in the bus, as illustrated in Fig. 1(a). As a result, the total intrinsic loss increases, leading to an overall reduction of Q_i. However, the presence of a common loss channel for the TE_{00} and TE_{10} modes allows for the creation of quasi-bound states in the continuum (quasi-BICs) at their Vernier frequencies [36]. This interaction gives rise to two hybrid modes, one of which has significantly reduced loss at the expense of the other, resulting in high Q_i resonant modes.

We characterize the cold cavity properties of this device using swept-wavelength interferometry [39]. This technique enables the retrieval of the amplitude and phase of every longitudinal mode, hence allowing to unambiguously identify their coupling regimes. The normalized transmission spectrum and the extracted Q factors shown in Fig. 1(b) exhibit periodic patterns with a period equal to 31 FSRs, where only a small number of cavity modes in the C + L optical band are strongly overcoupled with large Q_i, and therefore capable of supporting high squeezing generation. All other modes are characterized by a low Q_i, which suppresses their oscillation even for high-power twin-beams [35]. The generation of quasi-BICs also affects the coupling of the cavity modes to the bus, resulting in a periodic Q_e shifted by a few FSRs. However, Q_L follows the periodicity of Q_i, such that the strongly overcoupled modes are those with the highest Q_L, limiting the possible achievable θ and $S_{on\text{-}chip}$.

The central mode highlighted with the blue dashed line in Fig. 1(b) is used as the pump, at frequency $\omega_p = 2\pi \times 190.59$ THz. The first signal and idler modes appear at $\omega_s = 2\pi \times 187.48$ THz and $\omega_i = 2\pi \times 193.70$ THz, respectively, due to the position of the strongly overcoupled modes and the energy and momentum conservation that must be fulfilled by FWM. We calculate the overcoupling coefficients for these modes as $\theta_s = 0.934$ and $\theta_i = 0.939$. The difference in the Q factors, and consequently in θ, is the first source of squeezing degradation, as it represents different photon losses experienced by the two beams during propagation in the ring and in the bus-ring coupling. For this device, the idler has a lower intrinsic loss and almost the same coupling loss as the signal. Using the lowest overcoupling coefficient (θ_s) in Eq. (1), we estimate an on-chip intensity difference squeezing of $S_{on\text{-}chip} = 11.8$ dB. Such a high value provides increased resilience against the losses arising from the detection and possible on-chip operations.

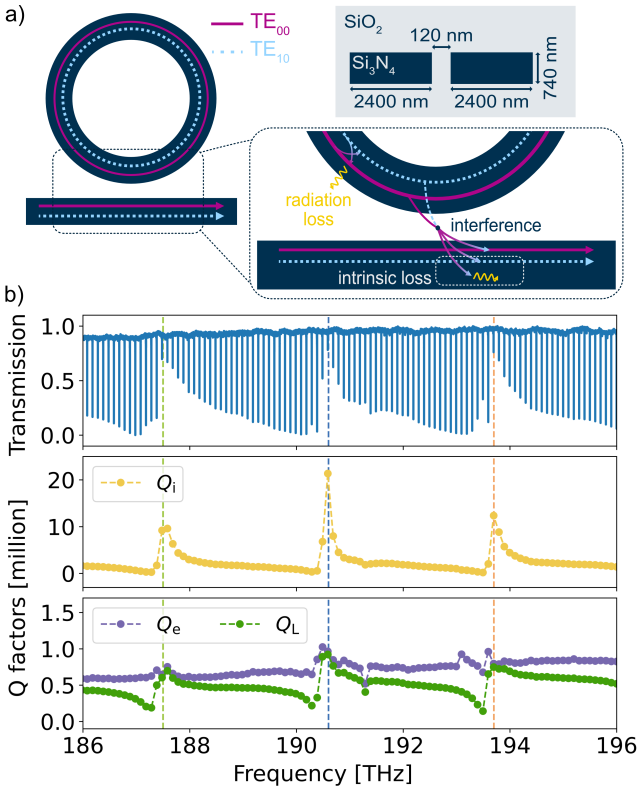

Fig. 1. (a) Schematic and cross-section of the microring resonator. The wide waveguides, combined with the small gap, allow quasi-BIC modes to arise. (b) Frequency-dependent periodic normalized transmission and Q factor distributions. The dashed lines indicate the strongly overcoupled resonances used as signal (green), pump (blue), and idler (orange).

From Eq. (1), we see that the detectable squeezing level strongly depends also on the setup losses and the quantum efficiency of the detector. To maximize η_{path}, we use free-space components to couple the light out of the chip and to separate the modes, as shown in the experimental setup in Fig. 2(a). In particular, an aspheric lens collects the output light, reducing the facet coupling loss to 0.8 dB compared to 2.98 dB of fiber-to-chip input loss. The 50 nm distance between the twin-beams, shown in Fig. 2(b), facilitates the spatial separation of the modes through a transmission grating, reducing the total number of free-space components necessary to send the signal and idler beams into the two ports of the balanced photodetector (BPD). During the noise measurement, it is crucial to balance the two PDs by equalizing their photocurrents, monitored on an oscilloscope via the DC output ports. Because of the unequal Q factors and the frequency-dependent losses of the components, the signal and idler powers are not identical. We correct this imbalance by intentionally increasing the path loss of the higher power beam. After that, the total path efficiency is $\eta_{path} = 0.46$, which includes the facet coupling loss, the losses from the free-space components, and the loss associated with coupling the beams into the small active area of the BPD. To characterize the quan-

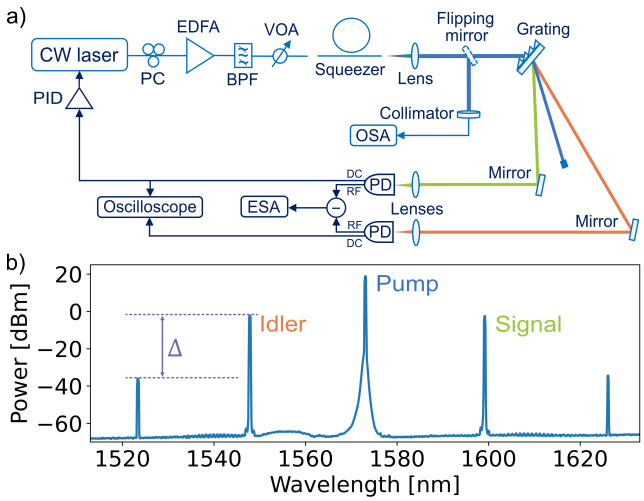

Fig. 2. (a) Simplified schematic of the intensity difference squeezing measurement setup. The different signal and idler paths after the grating are highlighted in green and orange, respectively. BPF, optical band pass filter; CW laser, continuous wave laser; EDFA, erbium doped fiber amplifier; ESA, electrical spectrum analyzer; OSA, optical spectrum analyzer; PD, photodetector; PID, proportional–integral–derivative control; VOA, variable optical attenuator. (b) Characteristic optical spectrum displaced to show the on-chip power. Here, the secondary mode suppression ratio Δ is about 33 dB.

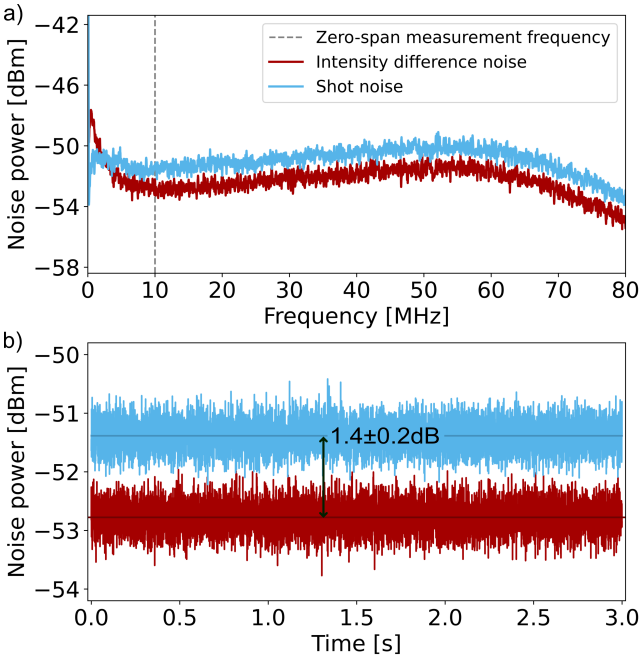

Fig. 3. (a) Comparison between the intensity difference noise power and the shot noise within the BPD bandwidth. Below 5 MHz, technical noise prevails over squeezing. (b) Zero-span measurement performed at 10 MHz. The signal and idler average on-chip power is 600 μW, and the measured squeezing level is 1.4 ± 0.2 dB. Data shown in (a) and (b) are collected using the ESA with a resolution bandwidth of 100 kHz and a video bandwidth of 3 kHz by averaging over 8 traces of 3 s each.

tum efficiency of the latter, we monitor the voltage at the RF common output port while sweeping the input power incident on each PD, one at a time. The curve slope, together with the nominal transimpedance gain, results in an average $\eta_D = 0.69$.

Figure 2(b) shows a typical output optical spectrum measured with the OSA, where the primary and secondary mode pairs are generated at the Vernier frequencies. In this case, the large suppression ratio of the secondary modes, $\Delta = 33$ dB, obtained at a twin-beam on-chip power of 600 μW, allows us to neglect their influence on the measured squeezing. By further decreasing the laser-pump resonance detuning, we generate signal and idler modes that can reach approximately 5 mW of on-chip power before cascaded FWM effects can no longer be neglected. However, such high twin-beam power is not reached during the actual squeezing measurement because of the saturation of the BPD.

Intensity difference squeezing is analyzed by comparing the noise power of the photocurrent difference generated in the BPD with the shot noise of the pump laser at frequency ω_p with a power equal to the average signal-idler power. We previously verified that the entire setup operates at the shot noise limit by measuring the linear dependence of the noise power on the input laser power. The noise spectra measured with the ESA are shown in Fig. 3(a). We observe squeezing across the entire BPD frequency bandwidth, starting from approximately 5 MHz. At lower frequencies, the technical noise from the laser and the BPD, as well as the additional noise due to the beam power imbalance, dominates over the detectable squeezing. The shape of the measured curves resembles that of the dark noise spectrum of the BPD, which remains below the measured shot noise. To accurately characterize the intensity difference squeezing level, we perform the zero-span measurement shown in Fig. 3(b). We choose $\Omega = 2\pi \times 10$ MHz to stay within the frequency range where Eq. (1) is valid. We directly measure $S_{meas} = 1.4 \pm 0.2$ dB of squeezing, mainly limited by the quantum efficiency of the PDs and the losses associated with focusing the beams in the BPD. The uncertainty in the squeezing measurement comes from the accuracy of the ESA. The consistency of this squeezing level throughout the measurement time of 24 s is ensured by the stabilization of the signal-idler power done through the PID control loop, which directly changes the pump laser wavelength.

From S_{meas}, η_{path}, and η_D measured previously, we can calculate the corresponding on-chip squeezing $S'_{on\text{-}chip}$ generated in the bus waveguide. We model the effect of the total setup loss $\eta = \eta_{path}\eta_D$ with the typical beam splitter relation [40]:

$$V_{meas} = \eta V_{on\text{-}chip} + (1-\eta)V_{vac}, \quad \textbf{(2)}$$

where we assume to have in one input port the variance of the on-chip squeezing $V_{on\text{-}chip}$ and in the other port the variance of the vacuum state V_{vac}, equal to 1 by definition. The variance of the measured squeezing is obtained at the output transmission port. We calculate $S'_{on\text{-}chip} = 10\log_{10}(V_{on\text{-}chip}) = 9.2 \pm 5.1$ dB, in agreement with the inferred $S_{on\text{-}chip}$ obtained from the analysis of the Q factors. The large uncertainty on $S'_{on\text{-}chip}$ is obtained from the error 3propagation analysis and is mainly due to the measurement uncertainty of the power values used to estimate η and the uncertainty of the measured squeezing level. The comparison between $S'_{on\text{-}chip}$ and S_{meas} highlights the nonlinear worsening effect of loss on the detectable squeezing level. Nevertheless, for integrated squeezing sources, the key result is the high level of on-chip squeezing enabled by our engineered microring design because of the strongly overcoupling regime reached in the pump, signal, and idler resonance modes. These results represent a high-record value of intensity difference squeezing generated on-chip in PICs.

According to Eq. (1), the intensity difference squeezing level remains constant for any mode power above P_{th}, in contrast to

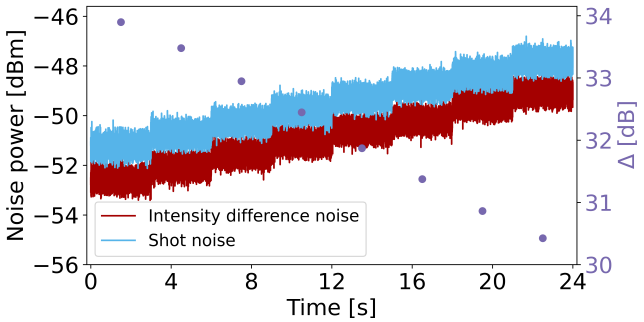

Fig. 4. Zero-span measurements of intensity difference squeezing performed while subsequently increasing the on-chip twin-beams average power from 480 μW to 1.07 mW by effectively changing the pump detuning. A constant squeezing level of 1.3 ± 0.2 dB is measured during the sweep, despite variations in the secondary mode suppression ratios Δ. The ESA settings are the same as for Fig. 3.

vacuum squeezing that reaches its maximum close to threshold [27]. Therefore, we investigate the stability of the squeezing generated from our device by sweeping the average signal and idler power. The results are shown in Fig. 4. In this measurement, the error signal used in the power stabilization feedback loop is gradually and continuously increased until an average twin-beam on-chip power of about 1 mW is reached, limited by the saturation of the BPD. During the sweep, the suppression ratio of the secondary modes decreases while remaining below 30 dB. The presence of these secondary modes has no evident effects on the squeezing level, which remains constant at 1.3 ± 0.2 dB over a total acquisition time exceeding 3 min. This demonstrates high stability over a large time scale and across a broad range of mode powers suitable for many sensing applications.

In summary, we demonstrate that quasi-BICs modes arising in an engineered Si_3N_4 microresonator enable access to the optimal coupling regime for high squeezing generation. We exploit these periodic strongly overcoupled resonances to generate twin-beam with an estimated record on-chip intensity difference squeezing of 11.8 dB, corresponding to a directly measured value of 1.4 ± 0.2 dB. We demonstrate the potential of this new design to provide a stable squeezing level over 3 min in a mode pair with a large wavelength separation. We observe that the relatively low power of the secondary mode pairs does not affect the squeezing level measured over a broad range of twin-beam power. This stability is also enabled by the overall low Q_i of the engineered device, which suppresses the oscillation in the other modes surrounding the signal and idler. Further improvements in the achievable on-chip intensity difference squeezing level can be obtained by further reducing the gap between the ring and the bus waveguides, thus increasing θ. As shown in [35], the enhancement of the overcoupling coefficient also allows higher signal and idler powers to be achieved. These improvements can be beneficial for several applications, especially in sensing, where stability and control over the twin-beams power and spectral separation can be critical.

Funding. Knut and Alice Wallenberg Foundation; Swedish Research Council (2020-00453, 2022-0657).

Acknowledgment. The device was fabricated at Myfab Chalmers.

Disclosures. The authors declare no conflicts of interest.

Data availability. Data underlying the results presented in this paper are available in Ref. [41].

REFERENCES

1. A. I. Lvovsky, *Squeezed Light* (John Wiley & Sons, Ltd., 2015), Chap. 5, pp. 121–163.
2. H. Aghaee Rad, T. Ainsworth, R. N. Alexander, *et al.*, Nature **638**, 912 (2025).
3. P. Marek, Phys. Rev. Lett. **132**, 210601 (2024).
4. B. J. Lawrie, P. D. Lett, A. M. Marino, *et al.*, ACS Photonics **6**, 1307 (2019).
5. H. Shi, Z. Chen, S. E. Fraser, *et al.*, npj Quantum Inf. **9**, 91 (2023).
6. D. Ganapathy, W. Jia, M. Nakano, *et al.*, Phys. Rev. X **13**, 041021 (2023).
7. W. Jia, V. Xu, K. Kuns, *et al.*, Science **385**, 1318 (2024).
8. G. Sim, H. Kim, and H. S. Moon, Sci. Rep. **15**, 7727 (2025).
9. M. Mehmet, S. Ast, T. Eberle, *et al.*, Opt. Express **19**, 25763 (2011).
10. K. Hirota, T. Kashiwazaki, G. Ha, *et al.*, "Generation of 10-db squeezed light from a broadband waveguide optical parametric amplifier with improved phase locking method," arXiv (2025).
11. H. Vahlbruch, M. Mehmet, K. Danzmann, *et al.*, Phys. Rev. Lett. **117**, 110801 (2016).
12. X. Shi, A. A. Baiju, X. Chen, *et al.*, "Squeezed light generation in periodically poled thin-film lithium niobate waveguides," arXiv (2025).
13. H. S. Stokowski, T. P. McKenna, T. Park, *et al.*, Nat. Commun. **14**, 3355 (2023).
14. V. D. Vaidya, B. Morrison, L. G. Helt, *et al.*, Sci. Adv. **6**, eaba9186 (2020).
15. Y. Zhao, Y. Okawachi, J. K. Jang, *et al.*, Phys. Rev. Lett. **124**, 193601 (2020).
16. Y. Zhang, M. Menotti, K. Tan, *et al.*, Nat. Commun. **12**, 2233 (2021).
17. A. E. Ulanov, B. Ruhnke, T. Wildi, *et al.*, Nat. Commun. **16**, 10791 (2025).
18. M. Jahanbozorgi, Z. Yang, S. Sun, *et al.*, Optica **10**, 1100 (2023).
19. Y. Shen, P.-Y. Hsieh, D. Srinivasan, *et al.*, "Highly squeezed nanophotonic quantum microcombs with broadband frequency tunability," arXiv (2025).
20. Z. Wang, K. Li, Y. Wang, *et al.*, Light Sci. Appl. **14**, 164 (2025).
21. X. Jia, C. Zhai, X. Zhu, *et al.*, Nature **639**, 329 (2025).
22. A. Dutt, K. Luke, S. Manipatruni, *et al.*, Phys. Rev. Appl. **3**, 044005 (2015).
23. A. Dutt, S. Miller, K. Luke, *et al.*, Opt. Lett. **41**, 223 (2016).
24. E. Brusaschi, M. Borghi, M. Bacchi, *et al.*, Opt. Quantum **2**, 214 (2024).
25. R. A. Kögler, G. C. Rickli, R. R. Domeneguetti, *et al.*, Opt. Lett. **49**, 3150 (2024).
26. Y. Shen, P.-Y. Hsieh, S. K. Sridhar, *et al.*, Optica **12**, 302 (2025).
27. Y. K. Chembo, Phys. Rev. A **93**, 033820 (2016).
28. N. Quesada, L. G. Helt, M. Menotti, *et al.*, Adv. Opt. Photonics **14**, 291 (2022).
29. M. A. Taylor, J. Janousek, V. Daria, *et al.*, Nat. Photonics **7**, 229 (2013).
30. C. A. Casacio, L. S. Madsen, A. Terrasson, *et al.*, Nature **594**, 201 (2021).
31. F. Li, T. Li, M. O. Scully, *et al.*, Phys. Rev. Appl. **15**, 044030 (2021).
32. T. Li, F. Li, X. Liu, *et al.*, Optica **9**, 959 (2022).
33. W. Yang, W. Diao, C. Cai, *et al.*, Chemosensors **11**, 18 (2022).
34. C. Wang, D. Hu, S. Zorzetti, *et al.*, "Squeezing enhanced sensing at an exceptional point," arXiv (2025).
35. Y. Sun, F. Lei, Y. Gao, *et al.*, Opt. Lett. **50**, 4798 (2025).
36. F. Lei, Z. Ye, K. Twayana, *et al.*, Phys. Rev. Lett. **130**, 093801 (2023).
37. Z. Ye, K. Twayana, P. A. Andrekson, *et al.*, Opt. Express **27**, 35719 (2019).
38. M. Girardi, Ó. B. Helgason, C. H. López-Ortega, *et al.*, Opt. Express **33**, 27451 (2025).
39. K. Twayana, Z. Ye, Ó. B. Helgason, *et al.*, Opt. Express **29**, 24363 (2021).
40. H.-A. Bachor and T. C. Ralph, *Squeezing Experiments* (John Wiley & Sons, Ltd., 2004), Chap. 9, pp. 232–309.
41. S. Persia, Y. Sun, V. Adya, *et al.*, "Intensity difference squeezing in a strongly overcoupled silicon nitride microresonator," Zenodo (2026), https://doi.org/10.5281/zenodo.18164363.